Supporting Information

Field-induced Ferromagnetism due to Magneto-striction in 1-D helical chain

Bikash Kumar Shaw,[a,‡] Mithun Das,[b,‡] Anik Bhattacharyya,[b] Biswa Nath Ghosh,[c] Susmita Roy,[d] Prabhat Mandal,[d] Kari Rissanen,[c] Shouvik Chattopadhyay,[b,*] Shyamal K Saha[a,*]

[a]Department of Materials Science, Indian Association for the Cultivation of Science, Kolkata -700 032,India.

[b]Department of Chemistry, Inorganic Section, Jadavpur University, Kolkata -700 032, India.

[c]Department of Chemistry, Nanoscience Center, University of Jyväskylä, P.O. Box 35, 40014 Jyväskylä, Finland

[d]Saha Institute of Nuclear Physics, 1/AF Bidhannagar, Calcutta 700 064, India

E-mail: cnssks@iacs.res.in ; shouvik.chem@gmail.com

Magneto-structural correlation

$$\chi_m = \frac{Ng^2\beta^2}{4kT} \cdot \left(\frac{1 + Ax + Bx^2 + Cx^3 + Dx^4 + Ex^5}{1 + Fx + Gx^2 + Hx^3 + Ix^3} \right)^{2/3} + N\alpha \quad \text{(S1)}$$

where, $x = J/kT$, A = 5.7979916, B = 16.902653, C = 29.376885, D = 29.832959, E = 14.036918, F = 2.7979916, G = 7.0086780, H = 8.6538644, I = 4.5743114 and the other constant terms have their usual meaning. $N\alpha$ is the temperature independent paramagnetism (TIP). Least-square fitting process gives the best-fit parameters of g = 2.06 (± 0.011), J = + 11.8 cm^{-1} (± 0.1) and $N\alpha$ = 5.8 x 10^{-5}emu mol^{-1} for **1** and g = 2.04 (± 0.018), J = + 0.75 cm^{-1} (± 0.02) and $N\alpha$ = 6.4 x 10^{-5}emu mol^{-1} for **2** respectively and the corresponding agreement factors, R^2= 5.3 x 10^{-5} and 5.9 x 10^{-5} $\left(\sum T^2(\chi_{obs} - \chi_{cal})^2 / \sum T^2(\chi_{obs})^2\right)$

The derivative plot of magnetization for complex **2** shown in Figure S9 indicates the absence of any ferromagnetic ordering at higher field unlike complex **1**.

ZFC-FC data at low magnetic fields (20 Oe) is also collected (Figure S10) which does not show any peak at low temperature region rather it shows the same behavior as that obtained at higher field (100 Oe).

We have measured the ac susceptibility as a function of temperature at several frequencies between 0.1 Hz to 51 Hz. A frequency dependence is observed in in-phase ac susceptibility behavior below 2.5K as shown in Figure S11. As our complex exhibits weak ferromagnetic exchange coupling in absence of magnetic field and ferromagnetic ordering appears under application of high field only, no prominent relaxation is observed in frequency response except splitting in real part of susceptibility data at low dc field (10 Oe).

Table S1: Crystal data and refinement details for **M** and **P** helices of complexes **1** and **2**.

Complex	**1M1**	**1M2**	**1M3**	**1P1**	**2M1**	**2M2**
Formula	$C_{16}H_{19}CuN_5O$	$C_{16}H_{19}CuN_5O$	$C_{16}H_{19}CuN_5O$	$C_{16}H_{19}CuN_5O$	$C_{16}H_{17}CuN_3O_2$	$C_{16}H_{17}CuN_3O_2$
Formula Weight	360.90	360.91	360.91	360.91	346.87	346.87
Temperature(K)	123	123	123	123	173	173
Crystal system	Orthorhombic	Orthorhombic	Orthorhombic	Orthorhombic	Orthorhombic	Orthorhombic
Space group	$P2_12_12_1$	$P2_12_12_1$	$P2_12_12_1$	$P2_12_12_1$	$P2_12_12_1$	$P2_12_12_1$
a(Å)	8.3103(3)	8.385(2)	8.3537(3)	8.3629(15)	6.9439(2)	7.032(12)
b(Å)	9.0566(5)	9.168(3)	9.1463(4)	9.1293(17)	7.7514(2)	7.827(14)
c(Å)	20.131(10)	20.215(6)	20.1898(8)	20.174(4)	27.5560(8)	27.76(5)
Z	4	4	4	4	4	4
d_{calc}(g cm^{-3})	1.582	1.543	1.554	1.556	1.553	1.508
μ(mm^{-1})	1.454	1.417	1.428	1.430	1.483	1.439
F(000)	748	748	748	748	716	716
Flack parameter	0.085(17)	-0.021(17)	0.004(13)	0.014(13)	-0.001(12)	0.012(16)
Total Reflections	7573	12855	13408	10013	4428	9390
Unique Reflections	3626	2296	3895	3081	2606	2860
Observed data [I > 2 σ (I)]	3097	2148	3349	2845	2512	2582
No. of parameters	209	208	208	208	201	199
R(int)	0.041	0.054	0.046	0.034	0.021	0.041
R1, wR2(all)	0.0561, 0.0862	0.0314, 0.0684	0.0438, 0.0779	0.0306, 0.0661	0.0261, 0.0605	0.0331, 0.0894
R1, wR2[I > 2σ(I)]	0.0439, 0.0821	0.0277, 0.0665	0.0333, 0.0734	0.0261, 0.0641	0.0243, 0.0592	0.0273, 0.0745

Table S2: Selected bond lengths (Å) for **M** and **P** helices of complex**es 1** and **2**.

	1M1	**1M2**	**1M3**	**1P1**	**2M1**	**2M2**
Cu(1)-O(1)	1.9071(18)	1.902(2)	1.898(17)	1.902(16)	1.9263(15)	1.932(4)
Cu(1)-N(1)	1.972(3)	1.970(3)	1.965(2)	1.968(2)	1.938(2)	1.951(4)
Cu(1)-N(2)	2.059(3)	2.059(3)	2.057(19)	2.057(19)	2.064(2)	2.073(5)
Cu(1)-N(3)	1.990(3)	1.986(3)	1.982(2)	1.984(2)	1.919(2)	1.927(5)
Cu(1)-N(5)[a]	2.418(3)	2.506(4)	2.501(3)	2.488(3)	-	-
Cu(1)-O(2)[b]	-	-	-	-	2.467(2)	2.522(5)

[a] = symmetry transformations: [#] = -1/2+x,1/2-y,2-z in **1M1**, [†] = -1/2+x,3/2-y,2-z in **1M2**, [‡] = 1/2+x,1/2-y,2-z in **1M3**, [≠] = 1/2+x,3/2-y,1-z in **1P1**.

[b] = symmetry transformations: [*] = -1-x, 1/2+y, -3/2-z in **2M1** and [$] = 1-x,-1/2+y,1/2-z in **2M2**.

Table S3: Selected bond angles (°) for **M** and **P** helices of complexes **1** and **2**.

	1M1	**1M2**	**1M3**	**1P1**	**2M1**	**2M2**
O(1)-Cu(1)-N(1)	91.43(10)	91.87(11)	91.44(8)	91.48(8)	90.52(8)	90.42(11)
O(1)-Cu(1)-N(2)	166.28(11)	167.66(11)	167.72(8)	167.52(8)	174.58(8)	174.52(11)
O(1)-Cu(1)-N(3)	90.45(10)	90.32(12)	90.59(9)	90.44(7)	91.68(9)	91.50(12)
O(1)-Cu(1)-N(5)[a]	99.51(10)	99.06(11)	98.97(8)	99.15(8)	-	-
O(1)-Cu(1)-O(2)[b]	-	-	-	-	92.84(7)	92.52(10)
N(1)-Cu(1)-N(2)	84.92(11)	84.61(11)	85.02(8)	84.92(8)	84.92(9)	84.71(11)
N(1)-Cu(1)-N(3)	164.47(13)	164.51(13)	164.83(11)	164.73(11)	172.42(11)	172.11(14)
N(1)-Cu(1)-N(5)[a]	100.24(11)	100.17(11)	99.97(10)	100.01(9)	-	-

N(2)-Cu(1)-N(3)	89.64(10)	90.11(12)	89.85(9)	89.98(8)	92.48(10)	92.99(12)
N(2)-Cu(1)-N(5)[a]	94.16(10)	93.21(11)	93.23(8)	93.25(8)	-	-
N(3)-Cu(1)-N(5)[a]	94.65(12)	94.64(13)	94.56(10)	94.64(10)	-	-
O(2)[b]-Cu(1)-N(1)	-	-	-	-	83.15(8)	83.44(10)
O(2)[b]-Cu(1)-N(2)	-	-	-	-	89.53(8)	89.44(10)
O(2)[b]-Cu(1)-N(3)	-	-	-	-	103.99(10)	104.11(13)

[a] = symmetry transformations: [#] = -1/2+x,1/2-y,2-z in **1M1**, [†] = -1/2+x,3/2-y,2-z in **1M2**, [‡] = 1/2+x,1/2-y,2-z in **1M3**, [≠] = 1/2+x,3/2-y,1-z in **1P1**.

[b] = symmetry transformations: [*] = -1-x, 1/2+y, -3/2-z in **2M1** and [$] = 1-x,-1/2+y,1/2-z in **2M2**.

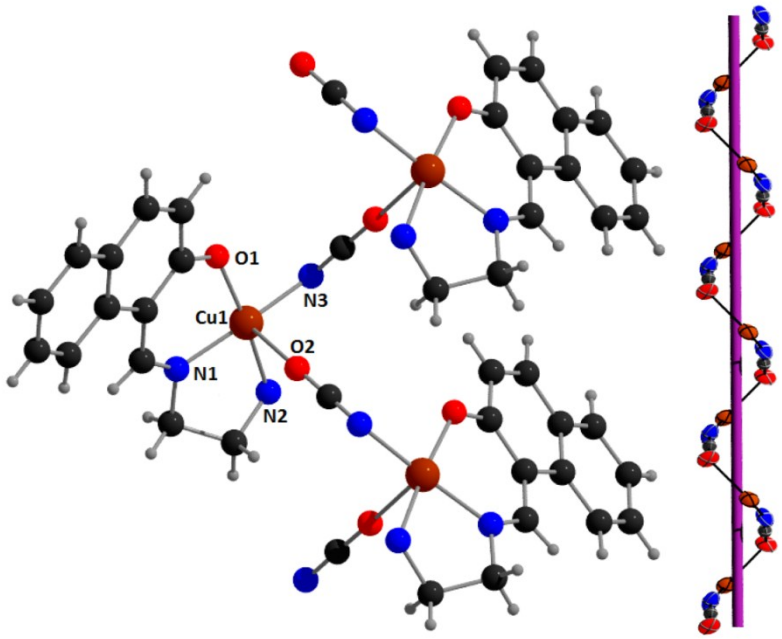

Figure S1: Perspective view of complex **2M1** with selective atom numbering scheme. Methyl groups of the amine nitrogen atoms have been omitted for clarity (left). A closer look to the M-helical chain (right).

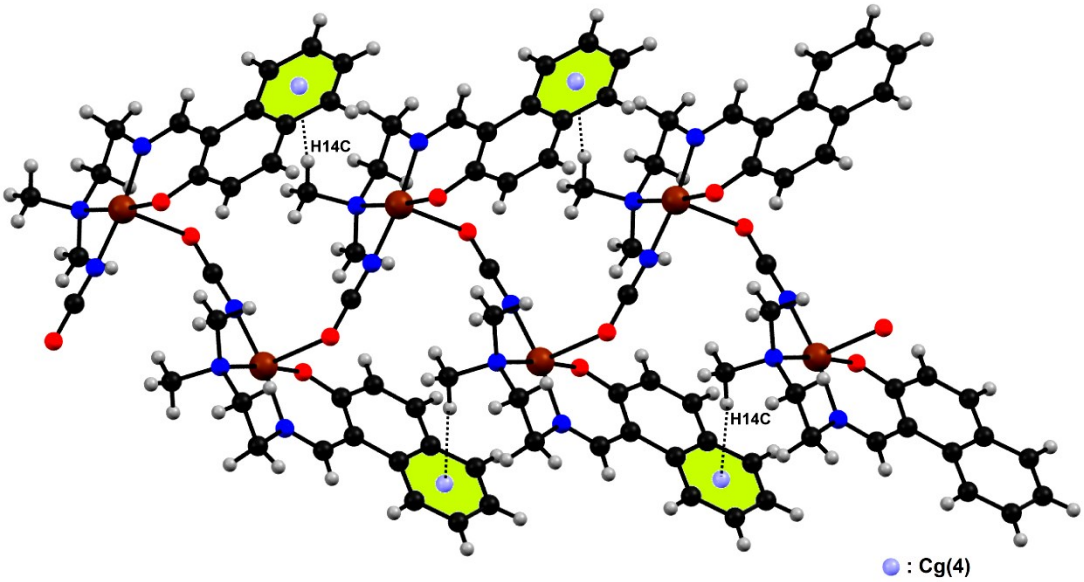

Figure S2: Intra-helix C–H···π interaction present in complex **2M1**.

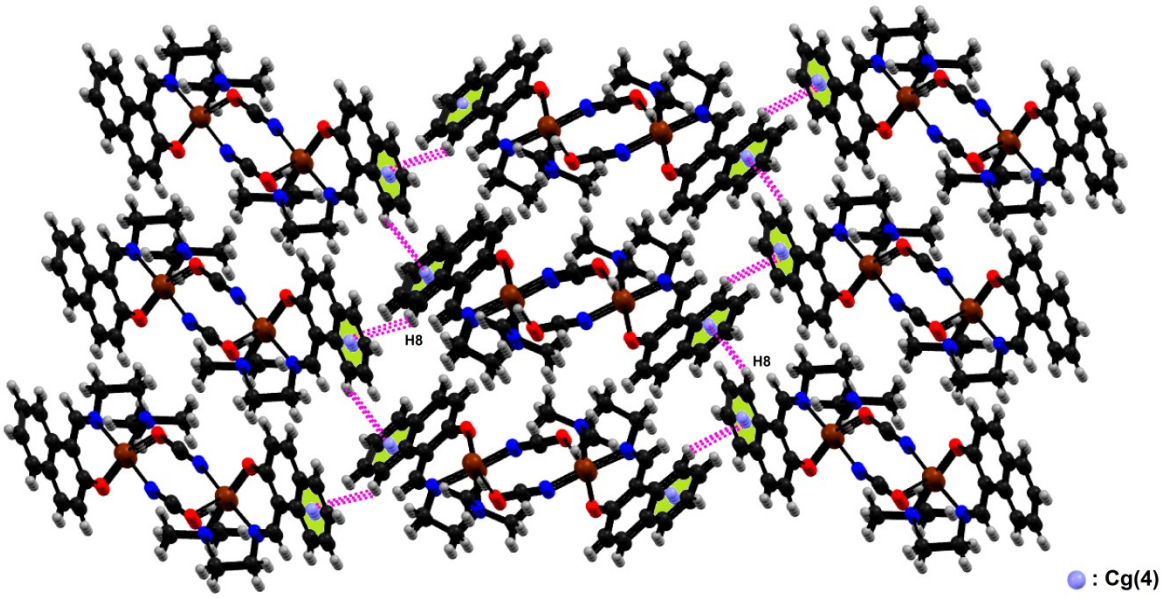

Figure S3: Inter-helix C–H···π interactions present in complex **2M1**.

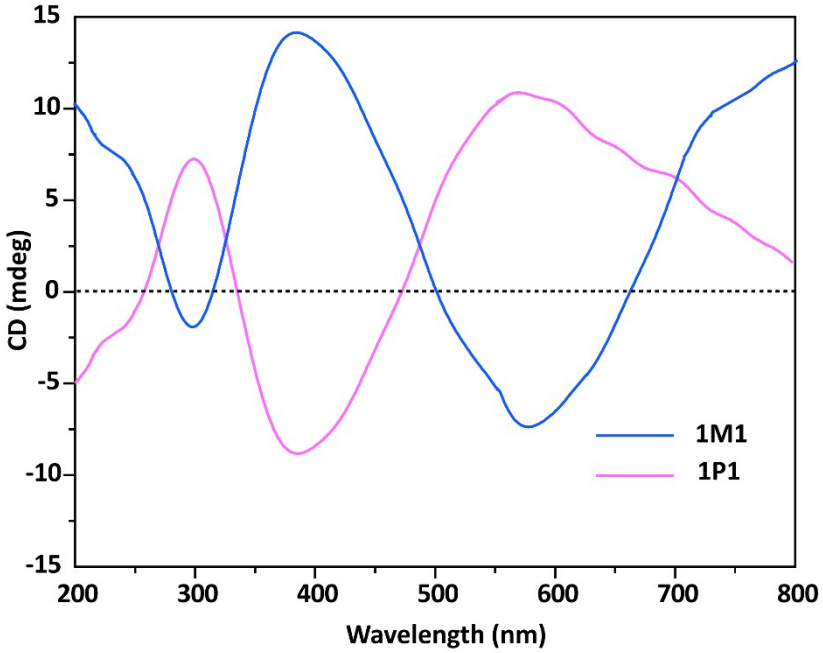

Figure S4: Solid state CD spectra of complex **1M1** and **1P1** at room temperature.

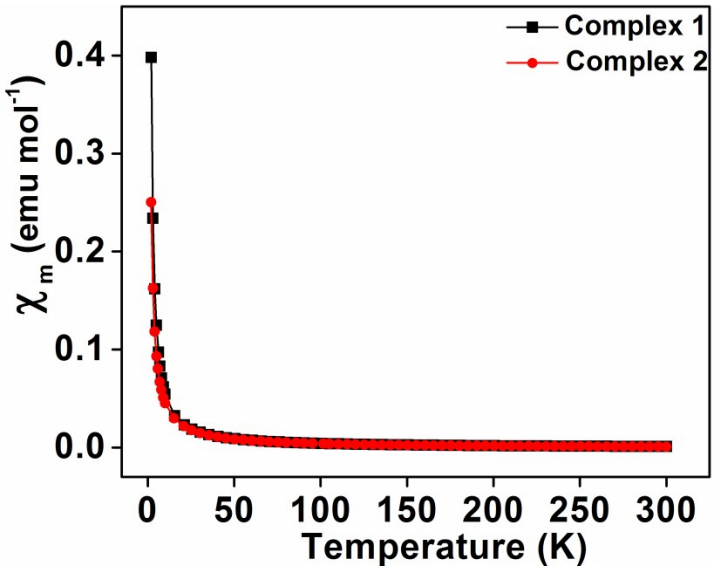

Figure S5: Change in molar susceptibility (χ_M) values with temperature for complexes **1** and **2**, measured at 100 Oe magnetic field.

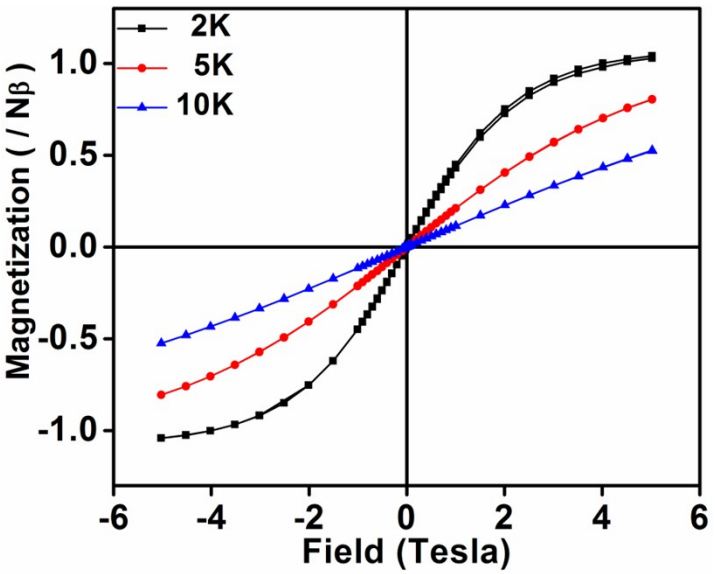

Figure S6: Variation of magnetization with magnetic field at different temperatures for complex **2**.

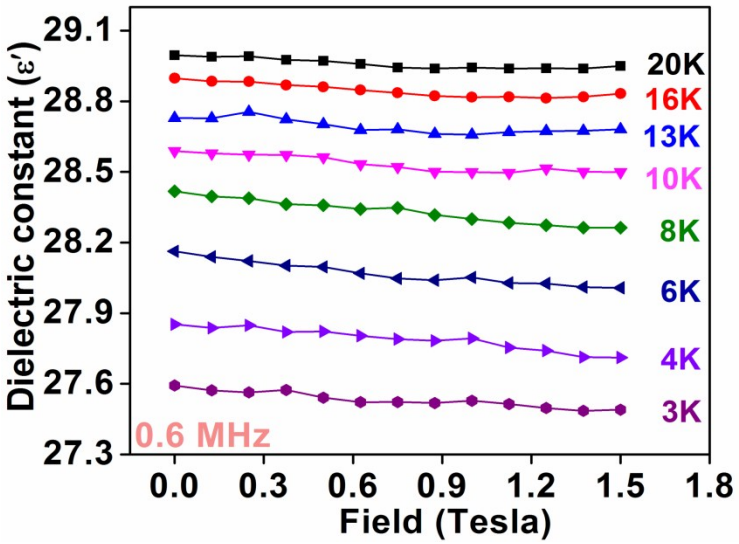

Figure S7: Variation of dielectric permittivity as a function of magnetic field at different temperatures for complex **2**. The dielectric permittivity values are shown for 0.6 MHz frequency.

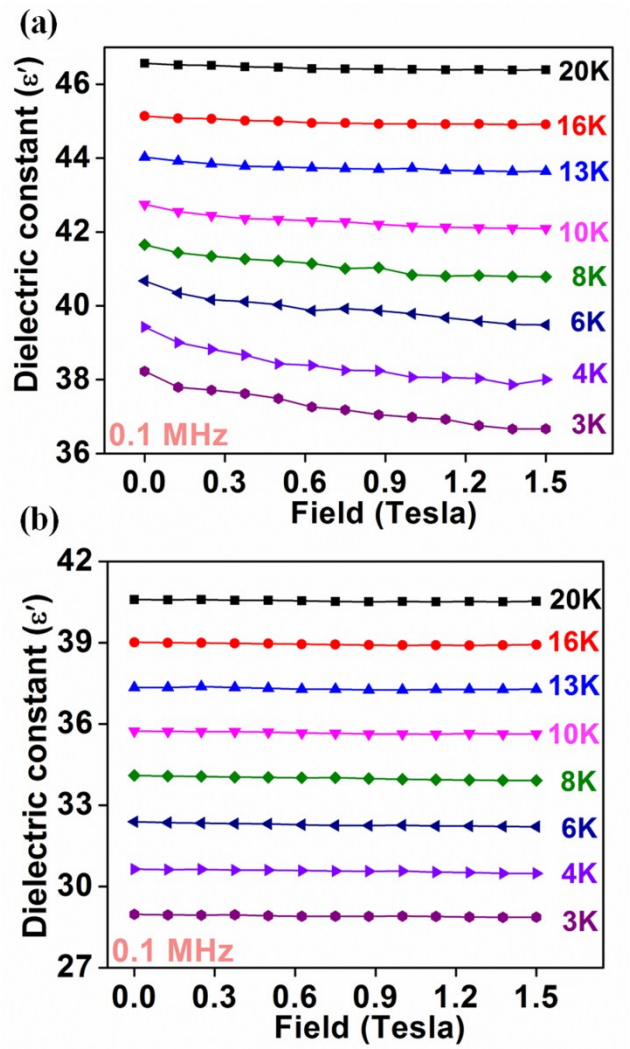

Figure S8: Variation of dielectric permittivity as a function of magnetic field at different temperatures for complex **1** (a) and complex **2** (b) respectively. The dielectric permittivity values are shown for 0.1 MHz frequency.

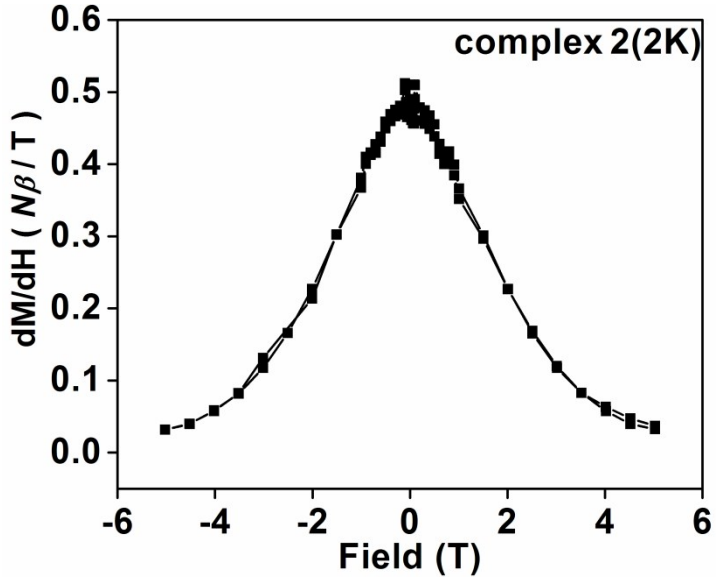

Figure S9: The derivative plot of magnetization for complex **2** reveals the absence of field induced ferromagnetism.

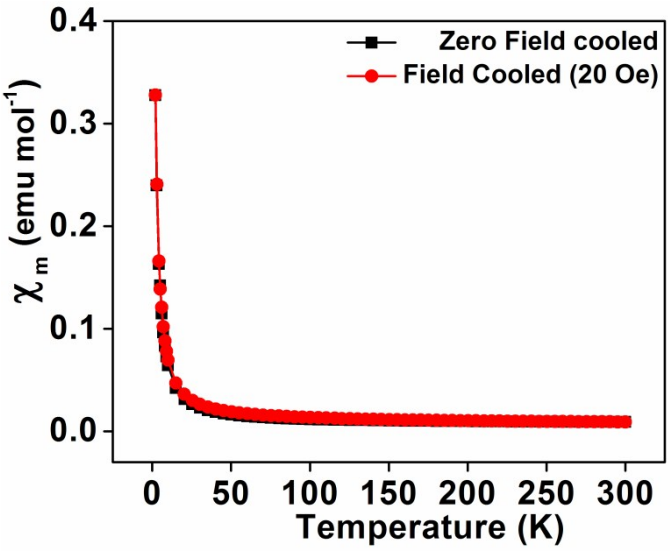

Figure S10: Change in molar susceptibility (χ_M) values with temperature for complexes **1**, measured at 20 Oe magnetic field.

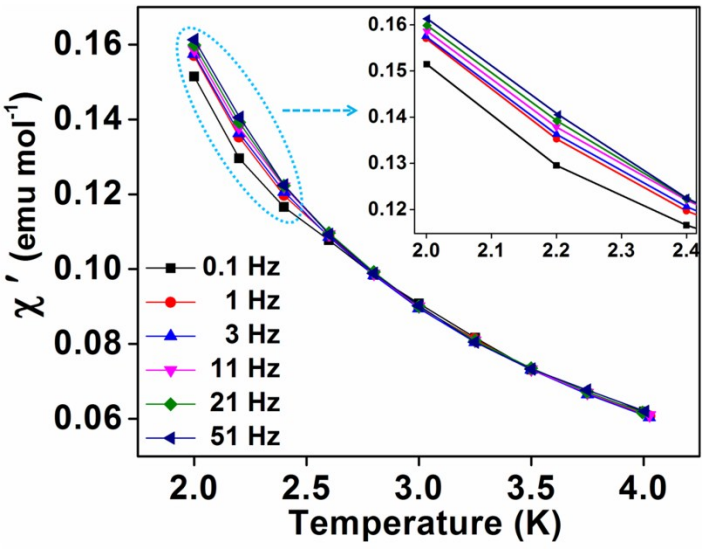

Figure S11: Variation of in-phase (χ') ac susceptibilities with temperature measured at 10 Oe dc field and 3 Oe ac oscillating field.